

Available online at www.sciencedirect.com

ScienceDirect

journal homepage: www.JournalofSurgicalResearch.com

Echocardiography allows for analysis of pulmonary arterial flow in mice with congenital diaphragmatic hernia



Mansi Shah, MD, Michael R. Phillips, MD, Megan Quintana, MD, Gary Stupp, RDCS, and Sean E. McLean, MD*

University of North Carolina, Chapel Hill, North Carolina

ARTICLE INFO

Article history:

Received 3 February 2017

Received in revised form

8 June 2017

Accepted 28 June 2017

Keywords:

Congenital diaphragmatic hernia

Pediatric surgery

Pulmonary hypertension

Echocardiography

ABSTRACT

Background: Congenital diaphragmatic hernia (CDH) is a structural birth defect associated with pulmonary hypoplasia and pulmonary arterial hypertension (PAH). We hypothesize that echocardiography provides a method to assess real-time right ventricle (RV) function, remodeling, and pulmonary artery (PA) flow.

Materials and methods: Slit3 wild-type (WT) ($n = 6$) and knockout (KO) ($n = 5$) mice were analyzed at 2–3 months of age. Mice were anesthetized using isoflurane. Echocardiography was performed to analyze left and right ventricular wall thickness, internal diameter (ID), and function. Color Doppler was used to analyze flow in the PA and across the tricuspid valve.

Results: There was significant RV dilation in the KO mice versus WT, with an average RVID of 1.99 mm versus 1.26 mm, respectively ($P = 0.007$). Flow in the PA of KO mice was altered compared to WT, with elevated PA velocity time indices, 30.68 mm versus 22.13 mm ($P = 0.012$), elevated PA peak velocities, 952.61 mm/s versus 628.73 mm/s ($P = 0.003$), and decreased pulmonary acceleration times, 8.94 ms versus 16.18 ms ($P = 0.002$), respectively. Pulmonary vascular resistance, calculated by measuring tricuspid regurgitation peak velocity and right ventricular outflow tract velocity time index, was increased in KO versus WT mice, 17.61 mm²/s versus 8.91 mm²/s ($P = 0.003$), respectively.

Conclusions: Slit3 KO mice with CDH show evidence of PAH and resultant RV dilation. Using direct cardiac puncture, elevated RV systolic pressures have been demonstrated in KO mice as evidence of PAH. Echocardiography allows direct analysis of the PA and real-time RV function without sacrifice of the mouse. This mode of evaluation allows longitudinal study in mice with PAH and CDH.

© 2017 Elsevier Inc. All rights reserved.

Introduction

Congenital diaphragmatic hernia (CDH) is a relatively common congenital disorder affecting approximately 1 in 3000

children. There is significant morbidity and mortality related to CDH, and 10%–35% of all CDH patients do not survive beyond the neonatal period. Of the survivors, 50% will have long-term morbidity.¹ Morbidity and mortality in CDH are

This material was presented, in part, at the 2015 American College of Surgeons Meeting.

* Corresponding author. Department of Surgery, Division of Pediatric Surgery, University of North Carolina, CB 7223, Chapel Hill, NC 27599. Tel.: +919 966 4643; fax: +919 843 2497.

E-mail address: sean_mclean@med.unc.edu (S.E. McLean).
0022-4804/\$ – see front matter © 2017 Elsevier Inc. All rights reserved.
<http://dx.doi.org/10.1016/j.jss.2017.06.080>

largely due to the pulmonary arterial hypertension (PAH) and pulmonary hypoplasia that affects most CDH patients. Studies have shown that more severe PAH is associated with worse survival.² No therapy exists for PAH in CDH because the mechanisms leading to the development of PAH in CDH have yet to be determined. Thus, CDH patients are managed with ventilator strategies and pharmacologic measures that are only supportive in nature.

Slit3 is part of the Slit family of genes with a number of functions, including axonal guidance, angiogenesis, axon attraction and repulsion, and cell chemotaxis. It is expressed in the mesothelium of the diaphragm during embryonic development. Slit3 knockout (KO) mice have been found to develop a diaphragmatic hernia at birth similar to the central (septum transversum) CDH in humans.³ Previous studies in humans with CDH have shown pathologic changes in the pulmonary arteries and veins, known as pulmonary vascular remodeling, that lead to the development of PAH.⁴ The Slit3 KO mouse is a unique mouse model for CDH because the mice are viable, which provides the unique opportunity to measure for changes consistent with PAH *in vivo*.

Current methods to evaluate PAH in mouse models include right heart catheterization and measurement of the right ventricular systolic pressure (RVSP), which in the absence of pulmonary stenosis allows for an estimation of PAH.⁵ However, right heart catheterization is a terminal procedure in mice, which precludes longitudinal study. Furthermore, right heart catheterization is difficult in Slit3 KO mice with CDH that often have distorted thoracic anatomy as a result of the diaphragmatic hernia. Therefore, assessment of RVSP by direct cardiac puncture has been performed in our laboratory to estimate PAH. However, this too results in sacrifice of the mouse. The aforementioned limitations result in an inability to serially assess PAH in mouse models and prevent the longitudinal assessment of mice with PAH before and after potential treatment modalities, inhibiting the investigation of the mechanisms leading to the development of PAH in CDH.

In humans, although right heart catheterization is required to confirm the diagnosis of PAH, echocardiography is a commonly used screening test, and the only noninvasive technique to follow the course of the disease.⁶ Furthermore, studies have shown that echocardiography can successfully assess pulmonary hypertension in rat and mouse models in a noninvasive manner.^{7,8} We hypothesize that transthoracic echocardiography provides a method to assess real-time right ventricle (RV) function, remodeling, and pulmonary artery (PA) flow in the Slit3 KO mouse model for CDH.

Methods

Slit3 WT and KO mice were bred and housed at our institutional animal facility under Institutional Animal Care and Use Committee protocol. Six WT and five KO mice were analyzed at 2-3 months (adult) of age, of which six mice were males and five mice were females. To perform transthoracic echocardiography, the mice were lightly anesthetized using isoflurane anesthesia. Inhaled isoflurane was administered at 3%

induction and 1%-1.5% maintenance. Once anesthetized, each mouse was placed in the supine position on a temperature-controlled mouse pad. Isoflurane was administered with a goal heart rate of 450-500 beats per minute. The mouse was restrained by taping all four limbs to the temperature-controlled mouse pad. A depilatory agent was then applied to the anterior chest to remove any hair. The mice were observed continuously while anesthetized and restrained during the echocardiography procedure. Clinical signs of deterioration included a dramatic slowing of heart rate less than 400 bpm, abnormal breathing patterns, or absent response to toe-pinch, any of which resulted in reduction of the isoflurane anesthesia.

Cardiac function was analyzed via echocardiography using the VisualSonics Vevo 2100 ultrasound machine (FUJIFILM VisualSonics, Inc, Toronto, Ontario, Canada). Aquasonic Gel (Parker Laboratories, Inc, Fairfield, NJ), kept in a gel heater, was applied to the anterior chest. The transducer probe (40 MHz, VisualSonics Model MS550D) was applied to the anterior chest first in a parasternal long axis view, with an approximately 30° angle counterclockwise, left of the parasternal line with the transducer notch pointing caudally⁸ (Fig. 1A). In this position, using the B mode setting of the ultrasound machine, a full view of the left ventricle (LV) in the parasternal long axis view can be obtained (Fig. 2). Once the left ventricle is clearly visualized, the ultrasound can be switched to M mode, the mode representing the movement of structures over time, with the indicator line positioned to go through the widest portion of the LV chamber, using the aorta as a landmark. This view can be saved via cine store on the ultrasound machine to be used to perform off-line calculations of heart rate, LV anterior and posterior wall thickness, LV internal diameter, LV ejection fraction, and LV fractional shortening (Fig. 2).

Next, the parasternal short axis view is obtained. The ultrasound is placed back in B mode, and the transducer probe is rotated 90° clockwise from the parasternal long axis view, to obtain the parasternal short axis view (Fig. 1B). The probe can be tilted gently toward the cranium to obtain a cross-sectional view of the heart at the level of the aortic valve. In this view, the right atrium can be seen, separated from the RV by the tricuspid valve (Fig. 3). Once this view is obtained, the ultrasound can be switched to the color Doppler mode. The pulse wave (PW)-line of the ultrasound, the line placed in the direction of flow, can be placed over the tricuspid valve to measure flow through the tricuspid valve. This can be used for off-line calculations of pulmonary vascular resistance (PVR), using the equation,

$$PVR = TR_{\max \text{ velocity}} / VTI_{RVOT}$$

where $TR_{\max \text{ velocity}}$ is the maximum velocity of tricuspid regurgitation (Fig. 4), divided by the velocity time integral of the right ventricular outflow tract, VTI_{RVOT} .⁹

A modified parasternal long axis view can be obtained to visualize blood flow through the PA. Beginning in the parasternal long axis view position, in B mode of the ultrasound, the probe can be gently rotated clockwise, until the probe is parallel to the sternum on the left hemithorax of the mouse. The probe can then gently be tilted laterally to obtain a view of the PA crossing over the aorta. Once this view is obtained in B

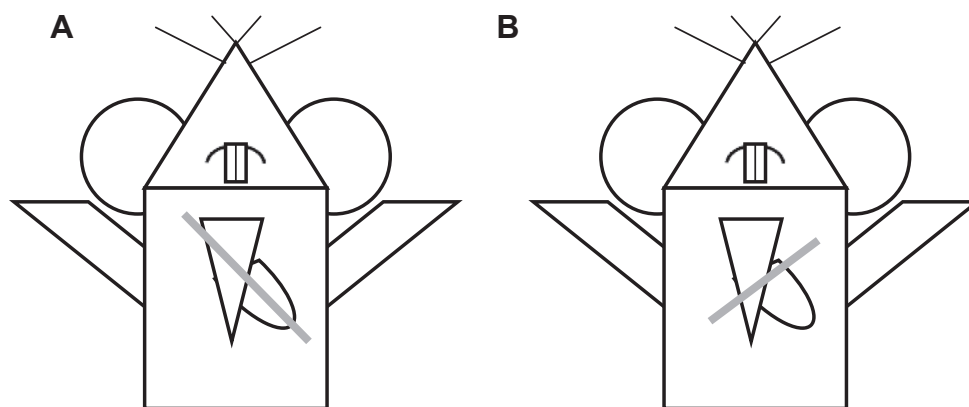


Fig. 1 – Illustration of probe positioning. Gray line indicates probe position to obtain the (A) parasternal long axis view and (B) parasternal short axis view.

mode, the ultrasound can be switched to the color Doppler mode. The PW line of the ultrasound can be placed along the PA, parallel to the direction of blood flow in the vessel, to obtain a flow waveform (Fig. 5). This can be repeated for flow across the pulmonary valve and for the flow through the right ventricular outflow tract. These views can be saved via cine store on the ultrasound and can be used to perform off-line calculations of PA velocity time index, PA peak flow velocity (Fig. 6), pulmonary valve velocity time index, and right ventricular outflow tract velocity time index. Mean pulmonary arterial pressure (MPAP) cannot be accurately calculated in the mouse using the Vevo 2100 ultrasound; therefore, the PA acceleration time (PAT) was used as an estimate of MPAP.¹⁰ The MPAP equation used in the Vevo 2100 ultrasound is based on human clinical equations, where the PAT is much higher than in the mouse, generally greater than 120 ms, due to the much lower human heart rate compared to the mouse. Therefore, the equation is inaccurate when applied to mice. PAT is used instead as an estimate of MPAP and is calculated by measuring the time between the initiation of the pulmonary arterial waveform and the pulmonary arterial peak velocity (Fig. 6) and is known to decrease as pulmonary arterial pressure increases⁵ and has been shown to inversely and linearly correlate with MPAP in humans.^{11,12}

Finally, the last view to be obtained is a modified parasternal short axis view. A similar angle is used to the parasternal short axis view (Fig. 1B); however, the probe is placed at the lateral aspect of the mid-right hemithorax to obtain a cross-sectional view of the heart with the RV anterior to the left ventricle (Fig. 7). Once this view is obtained in the B mode of the ultrasound, the ultrasound can be switched to M mode. The indicator line is then placed such that it transects the widest portion of the RV chamber. This view can be saved via cine store on the ultrasound to perform off-line calculations of RV anterior wall thickness, RV internal diameter (ID)—at diastole and at systole (Fig. 7), and RV fractional shortening (FS). RV FS is calculated using the equation,

$$\text{RV FS} = \left[\frac{(\text{RV}_{\text{end diastolic dimension}} - \text{RV}_{\text{end systolic dimension}})}{\text{RV}_{\text{end diastolic dimension}}} \right] \times 100$$

where the RV end diastolic dimension is calculated as the RVID at diastole, and the RV end systolic dimension is calculated as RVID at systole.¹³

To validate the echocardiographic findings, after echocardiography was performed, the RVSP of three WT and three KO mice was obtained by direct cardiac puncture. All mice were allowed to fully recover from the anesthesia

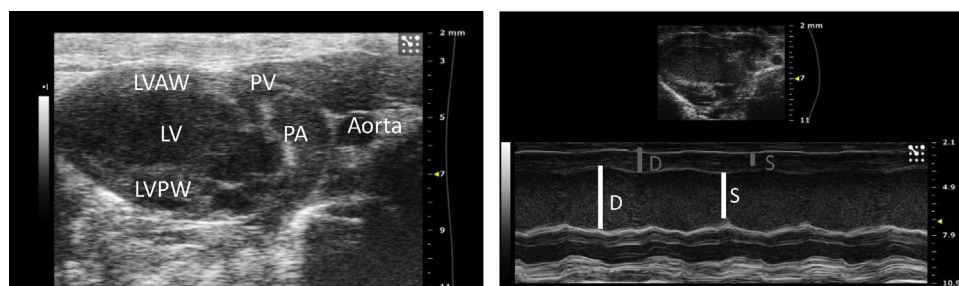


Fig. 2 – (Left) Parasternal long axis view of the left ventricle in B mode. LVAW = Left ventricle anterior wall, PV = pulmonary valve, PA = pulmonary artery, LV = left ventricle, LVPW = left ventricle posterior wall. (Right) Parasternal long axis view of the left ventricle in M mode. In the thumbnail above, the yellow dashed line represents the indicator line positioned at the widest portion of the LV chamber at the level of the aorta. In the M mode view below, measurements of the LV internal diameter (LVID) can be performed at diastole (D) and at systole (S), represented by the white lines. The LV anterior (LVAW) and posterior wall (LVPW) dimensions can also be calculated at diastole and systole, represented by the gray lines. (Color version of figure is available online.)

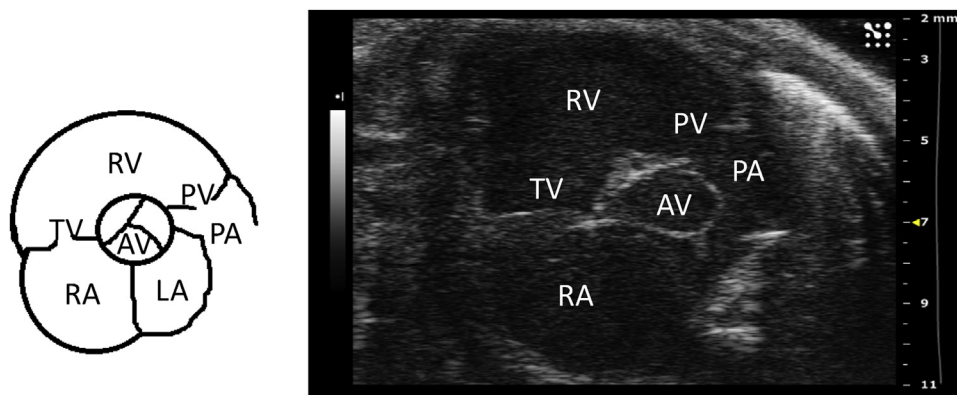


Fig. 3 – Parasternal short axis view at the level of the aortic valve. TV = tricuspid valve; RV = right ventricle; PV = pulmonary valve; AV = aortic valve; PA = pulmonary artery; RA = right atrium; and LA = left atrium. (Color version of figure is available online.)

administered during echocardiography. Inhaled isoflurane anesthesia was induced via the drop method, and then maintained via nose cone at 1%-2% isoflurane. Each mouse was placed on a temperature-controlled mouse pad, and all four limbs were restrained with tape. A 25-5/8 gauge needle attached to a pressure transducer was then inserted into the RV transdiaphragmatically. A right ventricular waveform was obtained and analyzed using LabChart6 software.

Off-line data analysis was performed using Vevo 2100 software. Statistical analysis was performed using t-test with Microsoft Excel. Male and female mice were used in this study, and the gender of the mouse was not considered to be a factor in the statistical analysis of the data. Echocardiography and off-line data analysis was performed by a single observer. The observer was blinded to the genotype of the mouse during off-line data analysis. This study was approved by the University of North Carolina Institutional Animal Care and Use Committee.

Results

WT and KO mice were approximately the same weight on average, 28.5 versus 28.8 kg, respectively ($P = 0.93$). Mean heart rate was similar in both groups, 470.49 versus 503.39 beats per minute (bpm), in WT versus KO mice respectively ($P = 0.54$). Left ventricular dimension and function was similar in WT versus KO mice, with LVAW (diastole) thickness of 0.82 versus 0.69 mm ($P = 0.07$), LVID (diastole) of 3.53 versus 3.46 mm ($P = 0.84$), LVPW (diastole) thickness of 0.96 versus 0.83 mm ($P = 0.29$), LV EF of 60.39 versus 58.66% ($P = 0.87$), and LV FS of 34.03 versus 30.75% ($P = 0.71$). For the aforementioned results please see [Table 1](#).

Right ventricular function was similar in WT versus KO mice, with RV FS of 39.19 versus 52.38% ($P = 0.19$) and right ventricular outflow tract (RVOT) VTI of 21.37 versus 17.30 mm ($P = 0.15$). However, the RV dimensions were significantly different in the two groups with a higher RVID (diastole) in KO mice compared

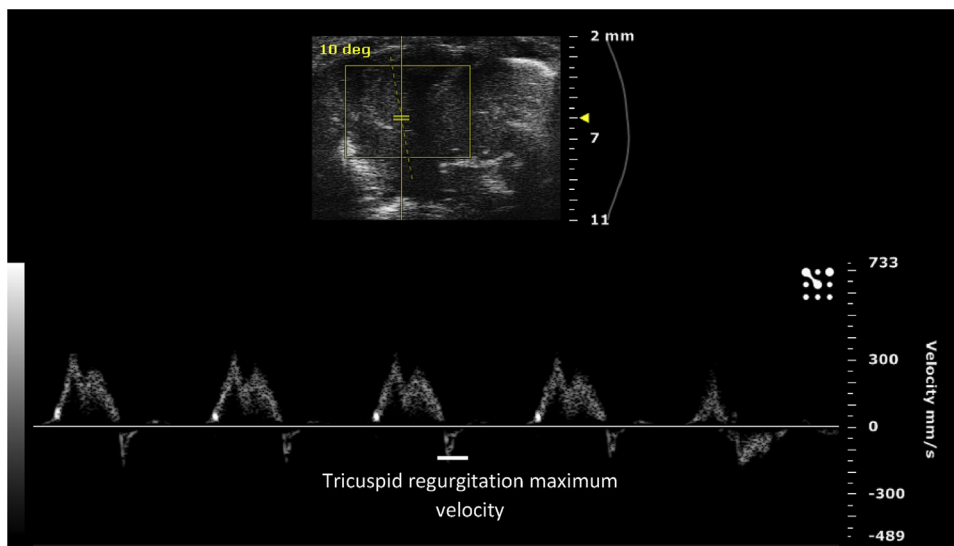


Fig. 4 – Tricuspid regurgitation maximum velocity, calculated from the color Doppler waveform of flow through the tricuspid valve. (Color version of figure is available online.)

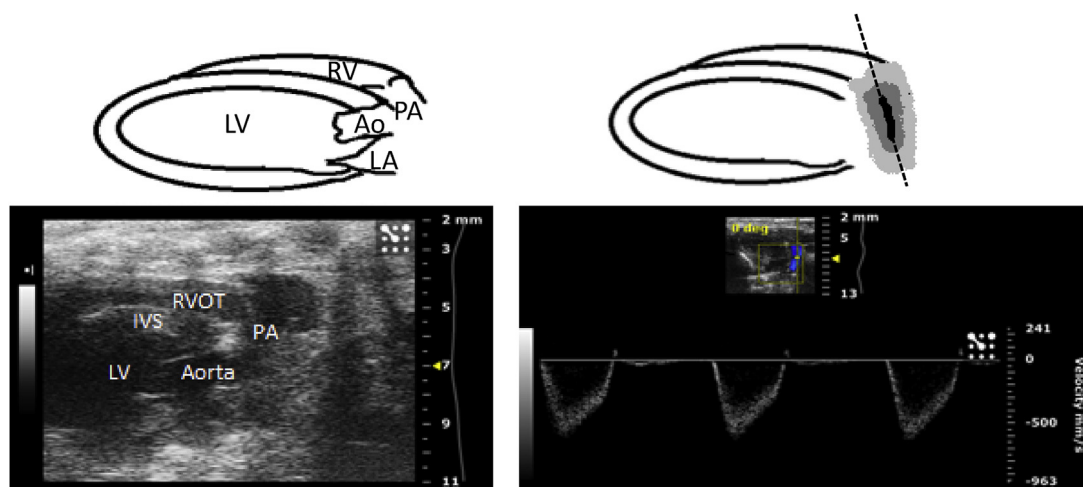


Fig. 5 – (Left) Modified parasternal long axis view demonstrating the right ventricular outflow tract and pulmonary artery in B mode of the ultrasound. (Right) Same view in color Doppler mode, used to assess flow through the pulmonary artery. The PW line is seen along the pulmonary artery on the right, positioned parallel to the direction of blood flow in the vessel, and can also be positioned to assess flow across the pulmonary valve and right ventricular outflow tract. RV = right ventricle; RVOT = right ventricular outflow tract; PA = pulmonary artery; LV = left ventricle; IVS = interventricular septum; Ao = aorta; and LA = left atrium. (Color version of figure is available online.)

to WT, 1.98 versus 1.26 mm, respectively ($P = 0.007$). RVAW (diastole) thickness was similar in both groups, 0.503 versus 0.500 mm in WT versus KO respectively ($P = 0.97$) (Table 1).

Flow through the PA was significantly altered in KO mice when compared to WT mice. The PA peak velocity was elevated in KO mice versus WT, 952.61 versus 628.73 mm/s, respectively ($P = 0.003$). PA VTI was also elevated in KO mice versus WT, 30.68 versus 22.13 mm, respectively ($P = 0.012$). PAT was decreased in KO mice versus WT, 8.94 versus 16.18 ms, respectively ($P = 0.002$), which suggests an estimated increased MPAP for KO compared to WT mice. Furthermore, pulmonary vascular resistance was increased in KO mice versus WT, 17.61 versus 8.91 mm²/s, respectively ($P = 0.003$) (Table 1).

To validate these echocardiographic findings, RVSP was calculated via direct cardiac puncture. The RVSP was significantly elevated in KO mice compared to WT mice, 35.39 ± 3.41 versus 16.01 ± 1.70 mmHg, respectively ($P = 0.0009$; Fig. 8).

Discussion

In this study, we are able to demonstrate that transthoracic echocardiography can accurately and reproducibly characterize PAH and resultant RV remodeling in Slit3 KO mice with CDH and PAH. Thus, we are able to assess PAH in a noninvasive manner that does not require sacrifice of the mouse. Before this method, studies of PAH relied largely on

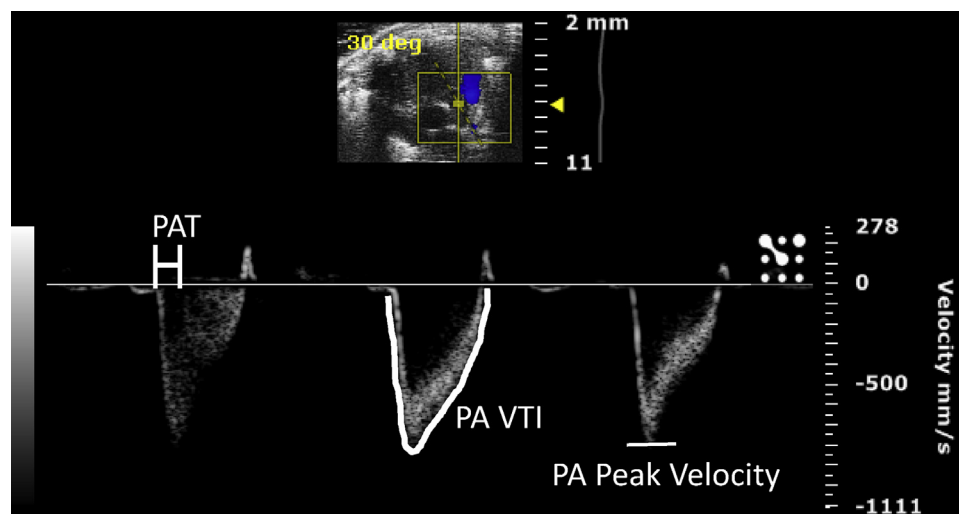


Fig. 6 – Color Doppler image of flow through the pulmonary artery (PA), used to calculate pulmonary arterial acceleration time (PAT), measured as the time elapsed between the beginning of the waveform to the point of PA peak velocity, PA velocity time integral (VTI), and PA peak velocity. (Color version of figure is available online.)

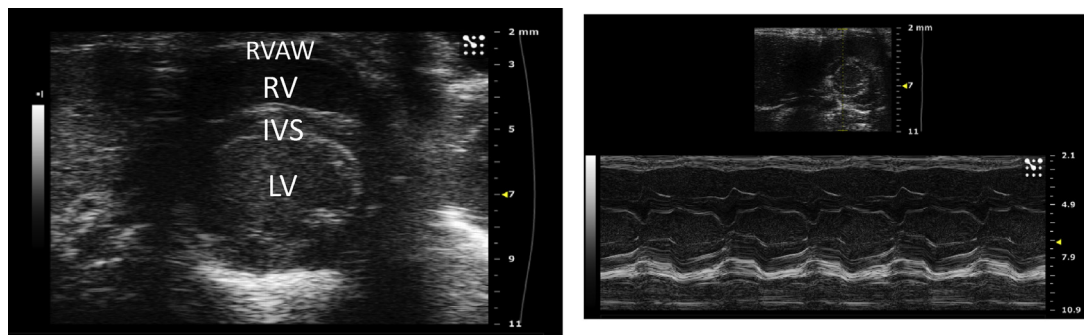


Fig. 7 – (Left) Modified parasternal short axis view in B mode visualizing the heart in cross section. The right ventricle is seen anterior to the left ventricle. (Right) Modified parasternal short axis view of the right ventricle in M mode. In the thumbnail above, the yellow dashed line represents the indicator line positioned at the widest portion of the RV chamber. In the M mode view below, measurements of the RV internal diameter (RVID) and RV anterior (RVAW) dimension can be calculated. RVAW = right ventricle anterior wall; RV = right ventricle; IVS = interventricular septum; LV = left ventricle. (Color version of figure is available online.)

estimation of PAH by obtaining RVSP measurement via right heart catheterization or direct cardiac puncture, both of which are nonsurvivable procedures. We also demonstrate the ability to validate our echocardiographic results with RVSP measurements obtained by direct cardiac puncture.

Table 1 – Echocardiographic measurements and RVSP calculated by direct cardiac puncture in WT and KO mice.

Measurements	WT (n = 6)	KO (n = 5)	P value
Weight (kg)	28.47	28.76	0.93
Heart rate (bpm)	470.49	503.39	0.54
LVAW diastole (mm)	0.82	0.69	0.07
LVID diastole (mm)	3.53	3.46	0.84
LVPW diastole (mm)	0.96	0.83	0.29
LV EF (%)	60.39	58.67	0.87
LV FS (%)	34.03	30.75	0.71
RV FS (%)	39.19	51.38	0.19
RVOT VTI (mm)	21.37	17.30	0.15
RVID diastole (mm)	1.26	1.99	0.007
RVAW diastole (mm)	0.503	0.500	0.97
PA peak velocity (mm/s)	628.73	952.61	0.0028
PA VTI (mm)	22.13	30.68	0.012
PAT (ms)	16.18	8.94	0.002
PVR (mm ² /s)	8.91	17.61	0.03
RVSP (mmHg)	16.01	35.39	0.0009
	WT (n = 3)	KO (n = 3)	

Bpm = beats per minute; LVAW = left ventricle anterior wall; LVID = left ventricle internal diameter; LVPW = left ventricle posterior wall; LV EF = left ventricle ejection fraction; LV FS = left ventricle fractional shortening; RVOT VTI = right ventricular outflow tract velocity time index; RVID = right ventricle internal diameter; RVAW = right ventricle anterior wall; PA VTI = pulmonary artery velocity time index; PAT = pulmonary artery acceleration time; PVR = pulmonary vascular resistance.

Slit3 KO mice do not exhibit changes in LV structure or function, with similar LVAW, LVPW, and LVID dimensions and LV EF and LV FS measurements to WT mice. Therefore, the presence of CDH does not appear to affect the left side of the heart in Slit3 KO mice, which is understandable given the knowledge that Slit3 KO mice with CDH develop central or right sided diaphragmatic hernias. Furthermore, although there is RV remodeling in Slit3 KO mice, with RV dilation, the RV function seems to be preserved, with similar RVOT VTI and RV FS measurements in KO and WT mice. The preserved RV function may account for the viability of the KO mice. Finally, we are able to demonstrate altered PA flow in a number of different ways, including significant differences in PA VTI, PA peak velocity, PAT, and PVR in KO compared to WT mice. These findings were validated by demonstrating elevated RVSP by direct cardiac puncture in the KO compared to WT mice.

Taken together, these echocardiographic techniques allow for a comprehensive assessment of PA flow and RV remodeling. PVR is able to be indirectly calculated, but PA flow is able

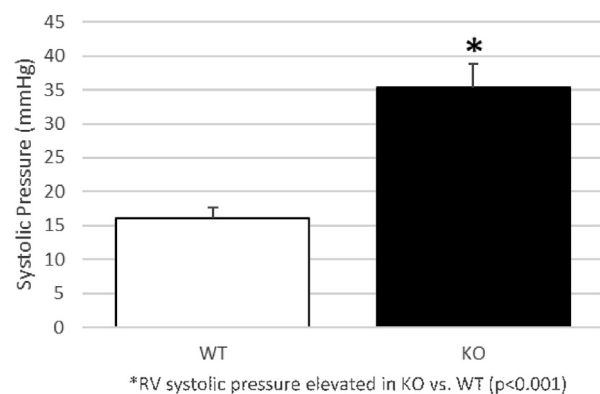


Fig. 8 – Right ventricular systolic pressure measured via direct cardiac puncture. RV systolic pressure is significantly elevated in KO compared to WT mice. *RV systolic pressure elevated in KO versus WT (P < 0.0001).

to be directly assessed by measuring PA VTI and PA peak velocity. Furthermore, although we were unable to accurately calculate MPAP, we were able to provide an estimate of MPAP by calculating PAT. Also, we were able to document the effect of ongoing PAH on the RV, by visualizing significant RV dilation.

As this noninvasive technique does not require sacrifice of the mouse, it provides a novel manner to longitudinally monitor the development of PAH in Slit3 KO mice with CDH. As we simultaneously work to understand the mechanisms driving the pulmonary vascular remodeling that causes PAH in CDH, echocardiography allows a method through which mice can be assessed over time to track the progression of PAH, and if possible, potentially monitor for reversal of PAH with appropriate treatment. Currently, there is limited information in the literature in general regarding right heart evaluation by echocardiography in the mouse, which through this study we demonstrate is indeed possible. Furthermore, the techniques described in this study can be used in a wider scope to investigate all murine models for pulmonary hypertension, further adding to the significance of this study.

A limitation to this method is that the mice required anesthesia. Fortunately, we have been able to limit the total procedural time to 10–15 min, minimizing the exposure of the mice to the anesthetic. We were also able to successfully anesthetize the mice with a low level of inhaled isoflurane, which has minimal cardiac side effects.¹⁴ The mice were also continuously monitored for evaluation of heart rate, breathing pattern, and response to toe-pinch, to assure that the mice were not deeply anesthetized. The heart rate in both groups of mice, WT and KO, were similar, suggesting an equivalent anesthetic effect that should not impede on echocardiographic measurements.

Conclusion

CDH is a relatively common congenital disorder with morbidity and mortality due to associated pulmonary hypoplasia and PAH. The Slit3 KO mouse model is a reliable model with which to study PAH in the context of CDH. Transthoracic echocardiography reliably and accurately is able to assess altered pulmonary arterial flow and resultant right ventricular remodeling in the Slit3 mouse model for CDH. This noninvasive method of assessment does not require sacrifice of the mouse and allows for a unique method to longitudinally study PAH in the context of CDH.

Acknowledgment

The authors would like to thank Dr Jennifer Whitham and Dr Scott Buck for their guidance in echocardiographic technique. The authors would also like to thank Dr. James Faber for technical assistance and overall guidance. They also would also like to greatly thank Maria Gambarian for her assistance in the care of the mice used in this study. This research was conducted under the aid of the UNC T32 Training Grant (grant

number T32GM008450) and the Robert Wood Johnson Harold Amos Faculty Development Program (67069).

Authors' contribution: M.S. (Mansi.Shah@unchealth.unc.edu) and S.E.M. (sean_mclean@med.unc.edu) contributed for conception, design, experimentation, analysis and interpretation, and writing of the manuscript. M.R.P., (miphilli@unch.unc.edu) M.Q., (Megan.Quintana@unchealth.unc.edu), and G.S. (gary_stupp@med.unc.edu) contributed for experimentation and revision of the manuscript.

Disclosure

The authors report no proprietary or commercial interest in any product mentioned or concept discussed in this article.

REFERENCES

1. Wynn J, Krishnan U, Aspelund G, et al. Outcomes of congenital diaphragmatic hernia in the modern era of management. *J Pediatr*. 2013;163:114–119.e1.
2. Dillon PW, Gilley RE, Mauger D, Zachary C, Meier A. The relationship of pulmonary artery pressure and survival in congenital diaphragmatic hernia. *J Pediatr Surg*. 2004;39:307–312. discussion 307–312.
3. Yuan W, Rao Y, Babiuk RP, Greer JJ, Wu JY, Ornitz DM. A genetic model for a central (septum transversum) congenital diaphragmatic hernia in mice lacking Slit3. *Proc Natl Acad Sci U S A*. 2003;100:5217–5222.
4. Taira Y, Yamataka T, Miyazaki E, Puri P. Adventitial changes in pulmonary vasculature in congenital diaphragmatic hernia complicated by pulmonary hypertension. *J Pediatr Surg*. 1998;33:382–387.
5. Thibault HB, Kurtz B, Raheer MJ, et al. Noninvasive assessment of murine pulmonary arterial pressure: validation and application to models of pulmonary hypertension. *Circ Cardiovasc Imaging*. 2010;3:157–163.
6. McLaughlin VV, Archer SL, Badesch DB, et al. ACCF/AHA 2009 expert consensus document on pulmonary hypertension: a report of the American College of Cardiology Foundation Task Force on Expert Consensus Documents and the American Heart Association: developed in collaboration with the American College of Chest Physicians, American Thoracic Society, Inc., and the Pulmonary Hypertension Association. *Circulation*. 2009;119:2250–2294.
7. Jones JE, Mendes L, Rudd MA, Russo G, Loscalzo J, Zhang YY. Serial noninvasive assessment of progressive pulmonary hypertension in a rat model. *Am J Physiol Heart Circ Physiol*. 2002;283:H364–H371.
8. Cheng HW, Fisch S, Cheng S, et al. Assessment of right ventricular structure and function in mouse model of pulmonary artery constriction by transthoracic echocardiography. *J Vis Exp*. 2014:e51041.
9. Abbas AE, Fortuin FD, Schiller NB, Appleton CP, Moreno CA, Lester SJ. A simple method for noninvasive estimation of pulmonary vascular resistance. *J Am Coll Cardiol*. 2003;41:1021–1027.
10. Granstam SO, Björklund E, Wikström G, Roos MW. Use of echocardiographic pulmonary acceleration time and estimated vascular resistance for the evaluation of possible pulmonary hypertension. *Cardiovasc Ultrasound*. 2013;11:7.
11. Martin-Duran R, Larman M, Trugeda A, et al. Comparison of Doppler-determined elevated pulmonary arterial pressure

- with pressure measured at cardiac catheterization. *Am J Cardiol.* 1986;57:859–863.
12. Kitabatake A, Inoue M, Asao M, et al. Noninvasive evaluation of pulmonary hypertension by a pulsed Doppler technique. *Circulation.* 1983;68:302–309.
 13. VisualSonics Inc.. *VisualSonics Vevo 2100 imaging system operator manual.* Toronto: VisualSonics Inc; 2001-2008.
 14. Constantinides C, Mean R, Janssen BJ. Effects of isoflurane anesthesia on the cardiovascular function of the C57BL/6 mouse. *ILAR J.* 2011;52:e21–e31.